K^+-proton partial-wave analysis to 3 GeV/c

Richard A. Arndt and L. David Roper
Department of Physics, Virginia Polytechnic Institute and State University, Blacksburg, Virginia 24061
(Received 30 October 1984)

Our K^+-proton analysis is extended to 3 GeV/c. Both energy-dependent and energy-band solutions are reported. The P_{13} resonance is still strongly present, and we find evidence of resonances in the D_{15} and P_{11} states. We describe our scattering analyses interactive dial-in (SAID) computing system, which allows other investigators to access the current data base and solutions for nucleon-nucleon, π-proton, and K^+-proton scattering.

I. INTRODUCTION

In our recent energy-dependent partial-wave analysis[1] we reported strong evidence for the existence of a P_{13} resonance pole at $(1796-i\,101)$ MeV. We have now extended the analysis to 3 GeV/c (2547-MeV laboratory kinetic energy and 2613-MeV center-of-mass total energy), doing both energy-dependent and energy-band analyses; and we have found that the P_{13} resonance is still strongly present, and it is accompanied by resonance poles in the D_{15} and P_{11} states. (We define "resonance poles" to be poles in the lower half plane on the "unphysical" or second sheet relative to the elastic-threshold cut, which poles are close enough to the real energy axis and strong enough to noticeably affect the physical amplitudes.) We also find zeros that accompany the poles; in the P_{11} case the zero determines the behavior along the real energy axis more than does the pole, and in the other two cases the zeros are connected with important behavior on the real energy axis.

Since our last K^+p scattering-analyses report,[1] we have been using a dial-in interactive computing facility [scattering-analyses interactive dial-in (SAID)] to communicate our latest results to other investigators. The usage level of SAID has been high, sometimes involving more than ten dial-ins per day from off-campus users into the VPI&SU computers. Some of these regular users requested that we transfer SAID to their local computers, which we have now done for many other sites with VAX computers in North America and Europe.

In the next section we describe the data used in the analysis, and in Sec. III we describe the energy-dependent parametrization used for the partial-wave amplitudes. Section IV describes the procedure used for obtaining the energy-dependent solution and energy-band solutions. Then Sec. V gives the results of the analysis, including the pole positions for the resonances. In Sec. VI we discuss the analytic structure of the partial-wave amplitudes in the complex energy plane, and in Sec. VII we consider possible future work for the K^+N system. Our SAID computing system is described in Sec. VIII.

II. DATA

Most of the data between 2 and 3 GeV/c are data reported in the same references as given in our previous work[1] for data below 2 GeV/c; there are three extra references[2] for data between 2 and 3 GeV/c. In addition to the α [Re$f(0)$/Im$f(0)$] "data" used in our previous analysis, we also used Martin's[3] Re$f(0)$ "data," but it has very little effect on the results. Data from the same references whose data were excluded in our 0—2-GeV/c analysis[1] were also excluded in this extended analysis. After pruning, 3663 data are used in this analysis. A plot of the angular data's availability is shown in Fig. 1.

III. PARAMETRIZATION

We first did the analysis using the parametrization of our previous work.[1] A large number of weak resonances occurred with that parametrization; in fact, essentially one in every partial wave. So another parametrization that has been proposed[4] was tried, and the resonance behavior was not as pronounced. As before, the parametrization allows for inelasticity in each partial wave by means of a single inelastic channel ($K^+\Delta$) involving an unstable particle (Δ), and resonance poles are not forced but can occur. However, now we use $K^+\Delta$ as the inelastic channel for all partial waves instead of using K^*N for the S_{11} state. This new parametrization accounts for threshold behavior in a different way than did our old parametrization.

The energy-dependent solution is parametrized through a coupled-channel K-matrix of the form

$$T=\rho^{1/2}\bar{T}\rho^{1/2}\,, \tag{1}$$

where

$$\bar{T}=K(1-CK)^{-1}=\text{reduced } T \text{ matrix}\,,$$

$$K=\begin{bmatrix} K_e & K_0 \\ K_0 & K_i \end{bmatrix}=\text{reduced } K \text{ matrix}\,,$$

$$C=\begin{bmatrix} C_e & 0 \\ 0 & C_i \end{bmatrix}\,,$$

and

$$\rho=\text{Im}C\,.$$

The reduced-K-matrix elements are parametrized as functions of energy as described in our previous work.[1]

In the above equations we have suppressed the orbital angular momentum, spin, and isospin indices. Now we

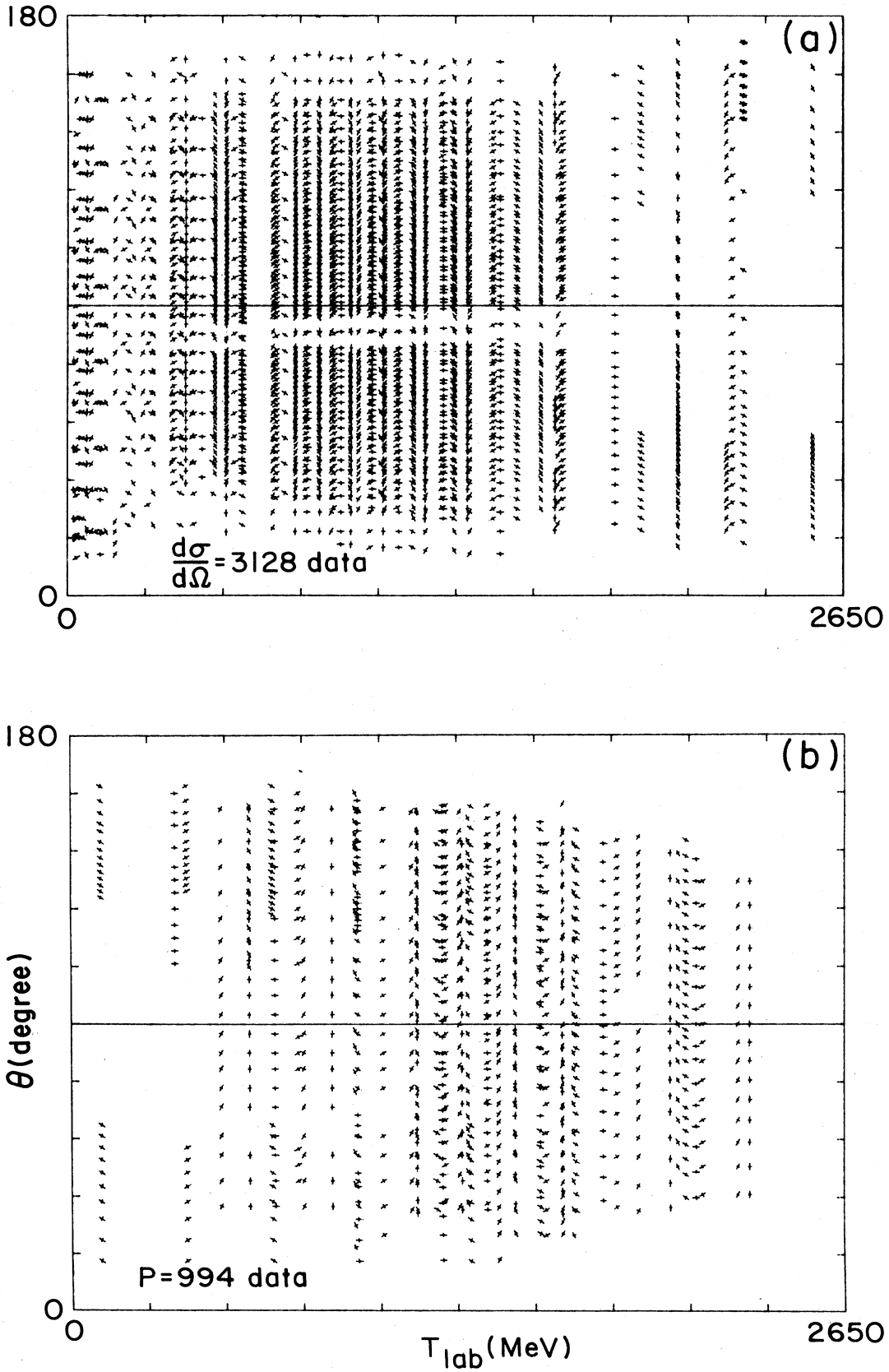

FIG. 1. Availability plot of K^+p angular data. (a) Differential cross section. (b) Polarization.

put the orbital angular momentum index on the dispersion function, C_l, which is given by

$$\pi C_l = \int_0^1 [x^{l+1/2}/(x-z)]dx \ , \tag{2}$$

a complex function, where

$$z=(W-W_t)/(W-W_z) \ ,$$

W = barycentric energy ,

$$W_t = \begin{cases} M_N+M_K & \text{(for the elastic channel } C_e) \ , \\ M_\Delta+M_K & \text{(for the inelastic channel } C_i) \ , \end{cases}$$

$$W_z = \begin{cases} M_N+M_K-150 & \text{(for the elastic channel } C_e) \ , \\ M_N+M_K+M_\pi & \text{(for the inelastic channel } C_i) \ , \end{cases}$$

and

$$M_\Delta = (1211-i51) \text{ MeV} = \Delta \text{ mass}$$

and the other masses are the usual ones. Thus, we are accounting for inelasticity by a single inelastic channel, $K^+\Delta$.

Now we drop the l index again. To ensure unitarity below the pion-production threshold, we require that

$$\text{Im}\, C_i = 0 \quad \text{for} \quad W < M_K+M_N+M_\pi \ . \tag{3}$$

The elastic component ($T_e = T_{11}$) of the T matrix can be written in the form

$$T_e = \rho_e \tilde{K}/(1-iC_e\tilde{K}) \ , \tag{4}$$

where

$$\tilde{K} = K_e + C_i K_0/(1-C_i K_i) \ .$$

The parametrization described above contains the dominant two-body unitarity cuts (KN,$K\Delta$), but does not contain the, generally weak, three-body cut ($KN\pi$). Since the integrals (C_e,C_i) can be calculated analytically for complex energy (W) (see the Appendix), the analytic continuation and interpretation of dominant singularities is simplified.

IV. FITTING PROCEDURE

We began with our 0—2-GeV/c solution[1] and moved toward 3 GeV/c by adding data in incremental 50-MeV laboratory-kinetic-energy ranges, adding extra parameters as needed to get a "good" fit at each step.

At the end we did energy-band analyses, starting from the energy-dependent solution, spaced 100 MeV apart with band widths of 200 MeV for energies above 800 MeV and spaced 50 MeV apart with band widths of 100 MeV for energies below 800 MeV. In these analyses we fixed the reduced-K-matrix [$\bar{T}$ in Eq. (1)] parameters that give energy dependence to have the energy-dependent values and varied the constant terms only.

Finally, we looked for resonance poles in each partial wave amplitude by making contour and three-dimensional plots of the square of the scattering amplitude versus the real and imaginary center-of-mass total energy (see Sec. VI).

V. RESULTS

The χ^2 for our fit to 3663 data is 4769. The angular observables are allowed to renormalize, weighted by the reported or estimated normalization errors.

The energy-dependent values for the partial-wave amplitudes are listed in Table I. The Argand plots for the energy-dependent solution are shown in Fig. 2. The partial waves for the energy-dependent solution and the energy-band solutions are shown together in Fig. 3.

The energy-band results agree reasonably well with the energy-dependent analysis. Our 0—3-GeV/c energy-dependent solution does not fit the inelastic cross section (Fig. 4) as well as does our previous 0—2-GeV/c solution[1] in the 700—1100-MeV energy range. Our parametrization does not appear to be flexible enough to allow for this rapid variation in the inelastic cut region that the data seem to demand, when we try to fit data over such a large energy range. Thus, the resonance pole positions given below for the P_{11} and P_{13} states are probably not highly accurate; the P_{13}'s position determined by our previous 0—2-GeV/c fit[1] may be more accurate.

The fits to the cross sections of our solution are shown in Fig. 4. We believe that the poorness of fit to the higher-energy inelastic cross sections are due to inconsistencies among that data, the total cross sections, and the differential cross sections. Our fitted curves are compared to some representative differential-cross-section data in Fig. 5 and to some representative polarization data in Fig. 6. It is easily seen that there are great inconsistencies among the different experiments and that there is perhaps a need for improvement of our fits.

VI. ANALYTIC STRUCTURE OF PARTIAL WAVES

The parametrization used in this analysis (see Sec. III and the Appendix) can be extrapolated into the complex plane to exhibit the analytic structure of the partial wave

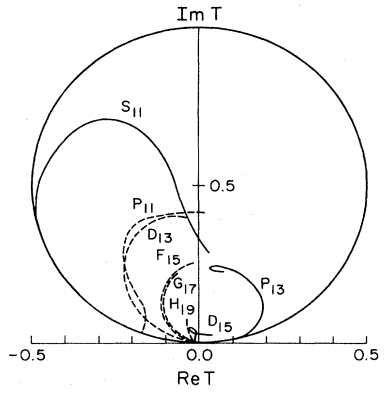

FIG. 2. Argand diagrams for our partial-wave amplitudes: The $j=l+\frac{1}{2}$ partial waves are solid curves and the $j=l-\frac{1}{2}$ partial waves are dashed curves.

TABLE I. Partial-wave amplitudes for energy-dependent fit.

(a) $J = L - \frac{1}{2}$ states

T_{lab}	$W_{c.m.}$	P_{11}		D_{13}		F_{15}		G_{17}		H_{19}		$I_{1,11}$		$J_{1,13}$	
(MeV)	(MeV)	ReT	ImT	ReT	ImT	ReT	ImT	ReT	ImT	ReT	ImT	ReT	ImT	ReT	ImT
50	1464	−0.015	0.000	−0.001	0.000	−0.000	0.000	0.000	0.000	−0.000	0.000	0.000	0.000	−0.000	0.000
100	1496	−0.037	0.001	−0.003	0.000	−0.001	0.000	0.000	0.000	−0.000	0.000	0.000	0.000	−0.000	0.000
150	1527	−0.062	0.004	−0.008	0.000	−0.002	0.000	0.001	0.000	−0.000	0.000	0.000	0.000	−0.000	0.000
200	1557	−0.086	0.007	−0.013	0.000	−0.003	0.000	0.001	0.000	−0.000	0.000	0.000	0.000	−0.000	0.000
250	1587	−0.109	0.012	−0.019	0.000	−0.005	0.000	0.002	0.000	−0.001	0.000	0.001	0.000	−0.000	0.000
300	1616	−0.130	0.018	−0.025	0.001	−0.007	0.000	0.002	0.000	−0.002	0.000	0.001	0.000	−0.000	0.000
350	1645	−0.147	0.022	−0.031	0.001	−0.009	0.000	0.003	0.000	−0.002	0.000	0.001	0.000	−0.001	0.000
400	1673	−0.158	0.026	−0.038	0.003	−0.012	0.000	0.003	0.000	−0.003	0.000	0.002	0.000	−0.001	0.000
450	1701	−0.159	0.032	−0.045	0.006	−0.015	0.001	0.003	0.001	−0.004	0.000	0.002	0.000	−0.001	0.000
500	1728	−0.151	0.049	−0.054	0.010	−0.017	0.001	0.002	0.001	−0.005	0.000	0.002	0.000	−0.001	0.000
550	1755	−0.149	0.080	−0.064	0.014	−0.020	0.002	0.001	0.002	−0.006	0.000	0.003	0.000	−0.002	0.000
600	1782	−0.157	0.112	−0.073	0.017	−0.023	0.003	−0.001	0.002	−0.007	0.000	0.003	0.000	−0.002	0.000
650	1808	−0.169	0.139	−0.083	0.021	−0.027	0.004	−0.002	0.002	−0.008	0.000	0.003	0.000	−0.002	0.000
700	1834	−0.180	0.162	−0.093	0.026	−0.031	0.005	−0.004	0.002	−0.009	0.000	0.003	0.000	−0.002	0.001
750	1859	−0.189	0.182	−0.103	0.031	−0.034	0.007	−0.005	0.003	−0.011	0.000	0.003	0.000	−0.002	0.001
800	1884	−0.196	0.200	−0.113	0.038	−0.038	0.009	−0.007	0.003	−0.012	0.000	0.003	0.000	−0.002	0.001
850	1909	−0.202	0.218	−0.123	0.044	−0.042	0.010	−0.010	0.003	−0.013	0.001	0.003	0.000	−0.002	0.001
900	1933	−0.206	0.234	−0.133	0.052	−0.046	0.013	−0.012	0.004	−0.014	0.001	0.002	0.000	−0.003	0.001
950	1957	−0.209	0.250	−0.143	0.060	−0.050	0.015	−0.014	0.004	−0.015	0.001	0.002	0.000	−0.003	0.002
1000	1981	−0.211	0.264	−0.153	0.069	−0.055	0.018	−0.017	0.005	−0.016	0.002	0.001	0.000	−0.003	0.002
1050	2005	−0.211	0.278	−0.163	0.078	−0.059	0.021	−0.020	0.006	−0.017	0.002	0.001	0.000	−0.003	0.002
1100	2028	−0.211	0.290	−0.172	0.089	−0.063	0.024	−0.023	0.007	−0.018	0.003	0.000	0.000	−0.003	0.003
1150	2051	−0.210	0.302	−0.181	0.100	−0.068	0.028	−0.026	0.008	−0.019	0.003	−0.000	0.000	−0.002	0.003
1200	2074	−0.208	0.313	−0.189	0.112	−0.072	0.032	−0.029	0.009	−0.020	0.004	−0.001	0.000	−0.002	0.004
1250	2096	−0.206	0.323	−0.197	0.124	−0.077	0.037	−0.033	0.010	−0.020	0.005	−0.002	0.000	−0.002	0.004
1300	2119	−0.203	0.333	−0.204	0.138	−0.081	0.042	−0.037	0.012	−0.021	0.006	−0.002	0.000	−0.002	0.004
1350	2141	−0.199	0.342	−0.210	0.151	−0.085	0.047	−0.040	0.013	−0.022	0.007	−0.003	0.000	−0.002	0.005
1400	2162	−0.195	0.350	−0.215	0.166	−0.089	0.053	−0.044	0.015	−0.023	0.008	−0.004	0.000	−0.002	0.005
1450	2184	−0.109	0.357	−0.220	0.180	−0.093	0.059	−0.048	0.017	−0.024	0.010	−0.005	0.000	−0.002	0.006
1500	2205	−0.185	0.364	−0.223	0.195	−0.097	0.066	−0.052	0.019	−0.024	0.011	−0.006	0.000	−0.002	0.006
1550	2226	−0.179	0.370	−0.225	0.211	−0.100	0.074	−0.057	0.022	−0.025	0.013	−0.007	0.000	−0.002	0.007
1600	2247	−0.173	0.375	−0.226	0.226	−0.103	0.082	−0.061	0.025	−0.026	0.015	−0.008	0.000	−0.002	0.007
1650	2268	−0.167	0.380	−0.226	0.242	−0.105	0.090	−0.065	0.028	−0.026	0.016	−0.009	0.000	−0.002	0.007
1700	2289	−0.160	0.385	−0.225	0.258	−0.107	0.099	−0.070	0.031	−0.027	0.018	−0.10	0.000	−0.002	0.008
1750	2309	−0.153	0.389	−0.222	0.273	−0.108	0.108	−0.074	0.035	−0.028	0.021	−0.011	0.000	−0.001	0.008
1800	2329	−0.146	0.393	−0.219	0.288	−0.109	0.118	−0.079	0.040	−0.028	0.023	−0.012	0.000	−0.001	0.009
1850	2349	−0.138	0.396	−0.213	0.302	−0.109	0.127	−0.084	0.044	−0.029	0.025	−0.013	0.000	−0.001	0.009
1900	2369	−0.130	0.399	−0.207	0.316	−0.108	0.137	−0.088	0.050	−0.029	0.028	−0.014	0.000	−0.001	0.010
1950	2389	−0.122	0.401	−0.200	0.329	−0.106	0.147	−0.092	0.056	−0.030	0.030	−0.015	0.000	−0.001	0.010
2000	2409	−0.114	0.403	−0.191	0.341	−0.103	0.158	−0.097	0.062	−0.031	0.033	−0.016	0.000	−0.001	0.010

TABLE I. (*Continued*).

T_{lab} (MeV)	$W_{c.m.}$ (MeV)	P_{11}		D_{13}		F_{15}		G_{17}		H_{19}		$I_{1,11}$		$J_{1,13}$	
		ReT	ImT	ReT	ImT	ReT	ImT	ReT	ImT	ReT	ImT	ReT	ImT	ReT	ImT
2050	2428	−0.105	0.405	−0.182	0.352	−0.100	0.168	−0.100	0.069	−0.031	0.036	−0.018	0.000	−0.001	0.011
2100	2447	−0.097	0.407	−0.171	0.362	−0.096	0.177	−0.104	0.077	−0.032	0.038	−0.019	0.000	−0.001	0.011
2150	2466	−0.088	0.409	−0.161	0.371	−0.091	0.187	−0.107	0.085	−0.032	0.042	−0.020	0.000	−0.000	0.012
2200	2485	−0.078	0.410	−0.149	0.378	−0.085	0.196	−0.110	0.094	−0.033	0.045	−0.021	0.000	−0.000	0.012
2250	2504	−0.069	0.411	−0.137	0.384	−0.078	0.204	−0.111	0.104	−0.034	0.048	−0.022	0.000	−0.000	0.013
2300	2523	−0.059	0.412	−0.125	0.388	−0.071	0.212	−0.112	0.114	−0.034	0.052	−0.023	0.001	−0.000	0.013
2350	2541	−0.050	0.413	−0.112	0.392	−0.063	0.220	−0.112	0.124	−0.035	0.056	−0.025	0.001	0.000	0.013
2400	2560	−0.040	0.414	−0.100	0.393	−0.055	0.226	−0.111	0.135	−0.035	0.059	−0.026	0.001	0.000	0.014
2450	2578	−0.030	0.415	−0.088	0.394	−0.047	0.232	−0.108	0.146	−0.036	0.063	−0.027	0.001	0.000	0.014
2500	2596	−0.020	0.416	−0.076	0.393	−0.038	0.237	−0.104	0.157	−0.037	0.067	−0.028	0.001	0.001	0.015
2550	2614	−0.010	0.417	−0.065	0.390	−0.029	0.242	−0.099	0.168	−0.037	0.071	−0.030	0.001	0.001	0.015
2600	2632	0.000	0.418	−0.054	0.387	−0.020	0.245	−0.092	0.179	−0.038	0.075	−0.031	0.001	0.001	0.015
2650	2650	0.010	0.419	−0.045	0.382	−0.010	0.248	−0.084	0.188	−0.039	0.079	−0.032	0.001	0.001	0.016

(b) $J=L+\frac{1}{2}$ states

T_{lab} (MeV)	$W_{c.m.}$ (MeV)	S_{11}		P_{13}		D_{15}		F_{17}		G_{19}		$H_{1,11}$		$I_{1,13}$		$J_{1,15}$	
		ReT	ImT	ReT	ImT	ReT	ImT	ReT	ImT	ReT	ImT	ReT	ImT	ReT	ImT	ReT	ImT
50	1464	−0.222	0.052	0.008	0.000	0.000	0.000	−0.000	0.000	−0.000	0.000	−0.000	0.000	−0.000	0.000	0.000	0.000
100	1496	−0.306	0.105	0.021	0.000	0.000	0.000	−0.000	0.000	−0.000	0.000	−0.000	0.000	−0.000	0.000	0.000	0.000
150	1527	−0.362	0.156	0.035	0.001	0.001	0.000	−0.000	0.000	−0.000	0.000	−0.000	0.000	−0.000	0.000	0.000	0.000
200	1557	−0.404	0.205	0.050	0.002	0.000	0.000	−0.000	0.000	−0.000	0.000	−0.000	0.000	−0.000	0.000	0.000	0.000
250	1587	−0.435	0.253	0.064	0.004	−0.000	0.000	0.000	0.000	0.000	0.000	−0.000	0.000	−0.000	0.000	0.000	0.000
300	1616	−0.458	0.298	0.079	0.006	−0.002	0.000	0.001	0.000	0.000	0.000	0.000	0.000	−0.001	0.000	0.000	0.000
350	1645	−0.474	0.342	0.095	0.009	−0.003	0.000	0.001	0.000	0.000	0.000	0.000	0.000	−0.001	0.000	0.000	0.000
400	1673	−0.484	0.382	0.111	0.013	−0.005	0.000	0.002	0.000	0.001	0.000	0.000	0.000	−0.001	0.000	0.000	0.000
450	1701	−0.489	0.419	0.130	0.019	−0.007	0.000	0.003	0.000	0.001	0.000	0.001	0.000	−0.001	0.000	0.001	0.000
500	1728	−0.488	0.453	0.151	0.031	−0.009	0.000	0.004	0.000	0.002	0.000	0.001	0.000	−0.002	0.000	0.001	0.000
550	1755	−0.483	0.486	0.171	0.051	−0.010	0.000	0.006	0.000	0.002	0.000	0.002	0.000	−0.002	0.000	0.001	0.000
600	1782	−0.473	0.517	0.185	0.079	−0.012	0.000	0.007	0.000	0.003	0.000	0.002	0.000	−0.002	0.000	0.001	0.000
650	1808	−0.461	0.548	0.189	0.111	−0.014	0.000	0.008	0.000	0.003	0.000	0.003	0.000	−0.002	0.000	0.001	0.000
700	1834	−0.448	0.576	0.183	0.141	−0.015	0.000	0.009	0.000	0.004	0.000	0.003	0.000	−0.002	0.000	0.002	0.000
750	1859	−0.433	0.602	0.171	0.165	−0.016	0.000	0.010	0.000	0.005	0.000	0.004	0.000	−0.002	0.001	0.002	0.000
800	1884	−0.417	0.624	0.155	0.184	−0.016	0.000	0.011	0.000	0.006	0.000	0.005	0.001	−0.002	0.001	0.002	0.000
850	1909	−0.400	0.644	0.140	0.197	−0.016	0.001	0.013	0.000	0.006	0.000	0.006	0.001	−0.002	0.001	0.002	0.000
900	1933	−0.382	0.662	0.125	0.206	−0.016	0.001	0.014	0.000	0.007	0.001	0.006	0.001	−0.001	0.001	0.003	0.000
950	1957	−0.363	0.676	0.112	0.213	−0.015	0.002	0.015	0.000	0.008	0.001	0.007	0.001	−0.001	0.001	0.003	0.000
1000	1981	−0.344	0.687	0.100	0.217	−0.014	0.003	0.015	0.000	0.009	0.001	0.008	0.001	−0.001	0.001	0.003	0.000
1050	2005	−0.324	0.696	0.089	0.220	−0.013	0.004	0.016	0.000	0.010	0.001	0.009	0.001	−0.001	0.002	0.003	0.001
1100	2028	−0.304	0.702	0.080	0.223	−0.011	0.006	0.017	0.000	0.011	0.001	0.010	0.002	−0.001	0.002	0.003	0.001

TABLE I. (*Continued*).

T_{lab}	$W_{c.m.}$	S_{11}		P_{13}		D_{15}		F_{17}		G_{19}		$H_{1,11}$		$I_{1,13}$		$J_{1,15}$	
(MeV)	(MeV)	ReT	ImT	ReT	ImT	ReT	ImT	ReT	ImT	ReT	ImT	ReT	ImT	ReT	ImT	ReT	ImT
1150	2051	−0.284	0.706	0.072	0.224	−0.008	0.009	0.018	0.000	0.012	0.001	0.011	0.002	−0.000	0.002	0.004	0.001
1200	2074	−0.264	0.707	0.066	0.226	−0.006	0.013	0.018	0.000	0.013	0.001	0.012	0.002	0.000	0.002	0.004	0.001
1250	2096	−0.244	0.705	0.060	0.226	−0.005	0.017	0.019	0.000	0.014	0.002	0.012	0.002	0.000	0.003	0.004	0.001
1300	2119	−0.225	0.702	0.055	0.227	−0.004	0.023	0.020	0.000	0.015	0.002	0.013	0.002	0.001	0.003	0.004	0.001
1350	2141	−0.207	0.696	0.051	0.228	−0.004	0.028	0.020	0.000	0.016	0.002	0.014	0.003	0.001	0.003	0.004	0.001
1400	2162	−0.190	0.688	0.047	0.228	−0.006	0.034	0.020	0.000	0.017	0.002	0.015	0.003	0.001	0.003	0.004	0.001
1450	2184	−0.173	0.678	0.044	0.228	−0.009	0.038	0.021	0.000	0.018	0.003	0.016	0.003	0.002	0.004	0.005	0.001
1500	2205	−0.158	0.666	0.042	0.228	−0.013	0.042	0.021	0.000	0.019	0.003	0.017	0.003	0.002	0.004	0.005	0.001
1550	2226	−0.143	0.653	0.040	0.228	−0.016	0.043	0.021	0.000	0.020	0.003	0.018	0.003	0.003	0.004	0.005	0.002
1600	2247	−0.130	0.639	0.038	0.228	−0.019	0.044	0.021	0.000	0.021	0.003	0.019	0.004	0.003	0.005	0.005	0.002
1650	2268	−0.118	0.624	0.037	0.228	−0.022	0.044	0.021	0.000	0.022	0.004	0.020	0.004	0.003	0.005	0.005	0.002
1700	2289	−0.106	0.607	0.037	0.228	−0.023	0.043	0.021	0.000	0.023	0.004	0.021	0.004	0.004	0.005	0.005	0.002
1750	2309	−0.096	0.590	0.036	0.227	−0.024	0.042	0.020	0.000	0.024	0.004	0.022	0.004	0.004	0.005	0.005	0.002
1800	2329	−0.087	0.572	0.037	0.227	−0.024	0.040	0.020	0.000	0.025	0.005	0.023	0.004	0.005	0.006	0.005	0.002
1850	2349	−0.078	0.554	0.037	0.227	−0.024	0.039	0.020	0.000	0.026	0.005	0.024	0.005	0.005	0.006	0.005	0.002
1900	2369	−0.070	0.536	0.038	0.226	−0.023	0.037	0.019	0.000	0.027	0.005	0.025	0.005	0.005	0.006	0.005	0.002
1950	2389	−0.062	0.517	0.039	0.226	−0.021	0.036	0.019	0.000	0.028	0.006	0.026	0.005	0.006	0.007	0.005	0.003
2000	2409	−0.055	0.498	0.040	0.225	−0.019	0.034	0.018	0.000	0.029	0.006	0.027	0.005	0.006	0.007	0.006	0.003
2050	2428	−0.048	0.480	0.041	0.225	−0.017	0.033	0.018	0.000	0.030	0.007	0.028	0.006	0.007	0.007	0.006	0.003
2100	2447	−0.042	0.461	0.043	0.224	−0.014	0.032	0.017	0.000	0.031	0.007	0.028	0.006	0.007	0.007	0.006	0.003
2150	2466	−0.035	0.443	0.045	0.224	−0.011	0.030	0.016	0.000	0.032	0.007	0.029	0.006	0.008	0.008	0.006	0.003
2200	2485	−0.028	0.425	0.047	0.223	−0.007	0.029	0.015	0.000	0.032	0.008	0.030	0.006	0.008	0.008	0.006	0.003
2250	2504	−0.021	0.407	0.049	0.223	−0.003	0.028	0.014	0.000	0.033	0.008	0.031	0.006	0.009	0.008	0.006	0.003
2300	2523	−0.013	0.390	0.052	0.222	0.000	0.028	0.014	0.000	0.034	0.009	0.032	0.007	0.009	0.009	0.006	0.003
2350	2541	−0.005	0.373	0.055	0.222	0.005	0.027	0.012	0.000	0.035	0.009	0.033	0.007	0.009	0.009	0.006	0.004
2400	2560	0.003	0.357	0.057	0.221	0.009	0.026	0.011	0.000	0.036	0.009	0.034	0.007	0.010	0.009	0.006	0.004
2450	2578	0.012	0.341	0.060	0.221	0.014	0.026	0.010	0.000	0.037	0.010	0.035	0.007	0.010	0.009	0.006	0.004
2500	2596	0.022	0.326	0.064	0.220	0.018	0.025	0.009	0.000	0.038	0.010	0.036	0.007	0.011	0.010	0.006	0.004
2550	2614	0.033	0.312	0.067	0.219	0.023	0.025	0.008	0.000	0.039	0.011	0.037	0.008	0.011	0.010	0.006	0.004
2600	2632	0.044	0.298	0.070	0.219	0.029	0.024	0.006	0.000	0.040	0.011	0.038	0.008	0.012	0.010	0.006	0.004
2650	2650	0.056	0.286	0.074	0.218	0.034	0.024	0.005	0.000	0.040	0.012	0.039	0.008	0.012	0.010	0.006	0.004

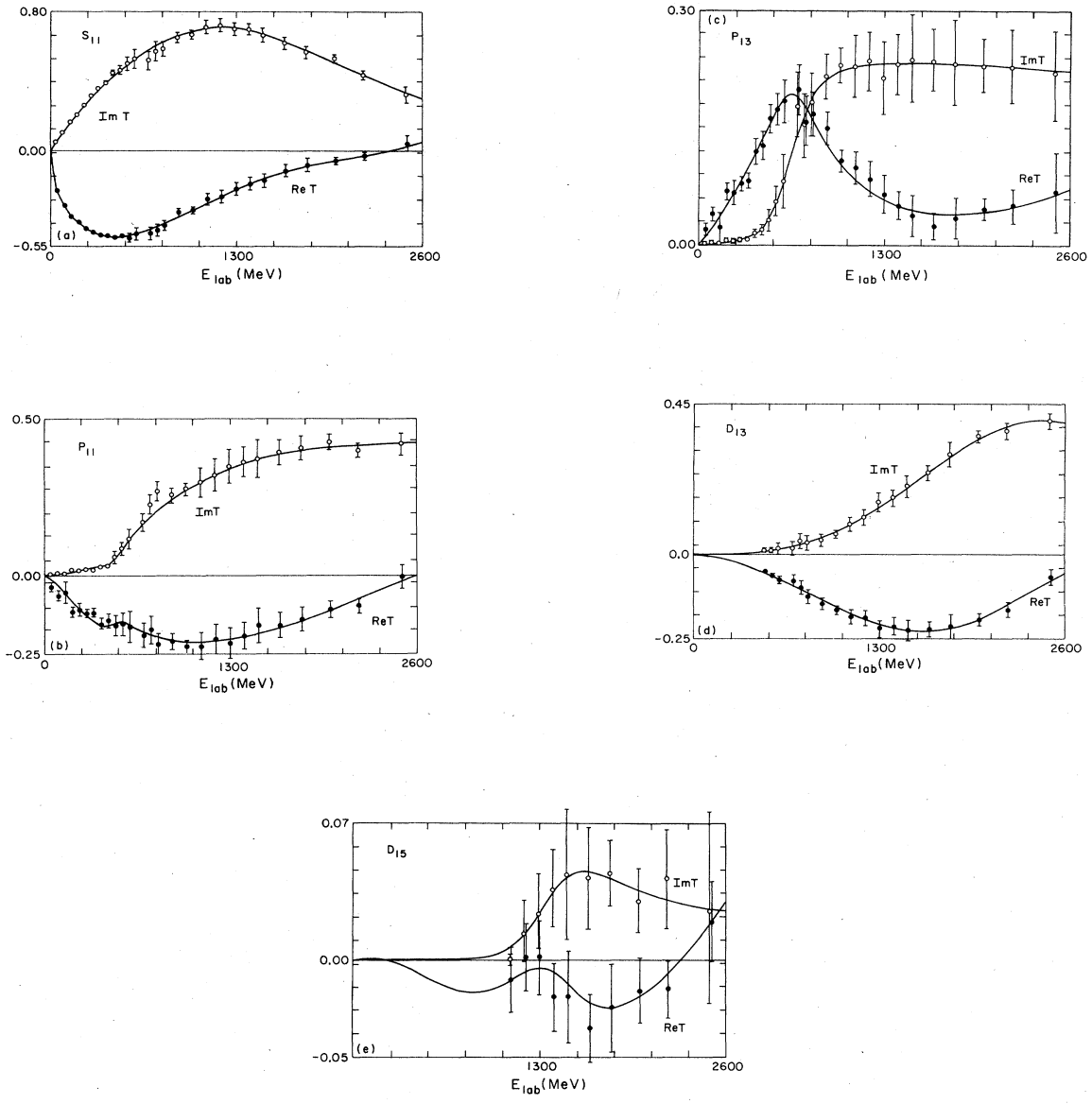

FIG. 3. Partial-wave scattering amplitudes. Solid curves are the energy-dependent solution and points with error bars are energy-band solutions.

amplitudes. Of particular interest is the possible existence of poles in the lower half plane on the second sheet relative to the elastic threshold cut, which are close enough to the real axis and strong enough to noticeably affect the physical amplitudes. We now discuss the results of such an extrapolation.

We again[1] find a resonance pole in the P_{13} state and we also find poles in the D_{15} and P_{11} states. The Argand diagrams for these three states are shown in Figs. 2, 7(a), 8(a), and 9(a). The resonance poles we find are at the following positions:

P_{13}, $(1780-i140)$ MeV ;

P_{11}, $(1725-i61)$ MeV ;

D_{15}, $(2161-i160)$ MeV .

As explained above, our previous result[1] for the P_{13} pole, $(1796-i101)$ MeV, may be more accurate than this result. We regard the evidence as strong for the P_{13} resonance and the existence of the other two resonance poles reported here to be highly probable. However, we expect further analyses with better data and/or parametrizations will considerably change the positions of all of these resonance poles. Therefore, we have made no attempt to assign errors to the pole-position values.

Each of the above poles is accompanied by a nearby zero. The minima are at

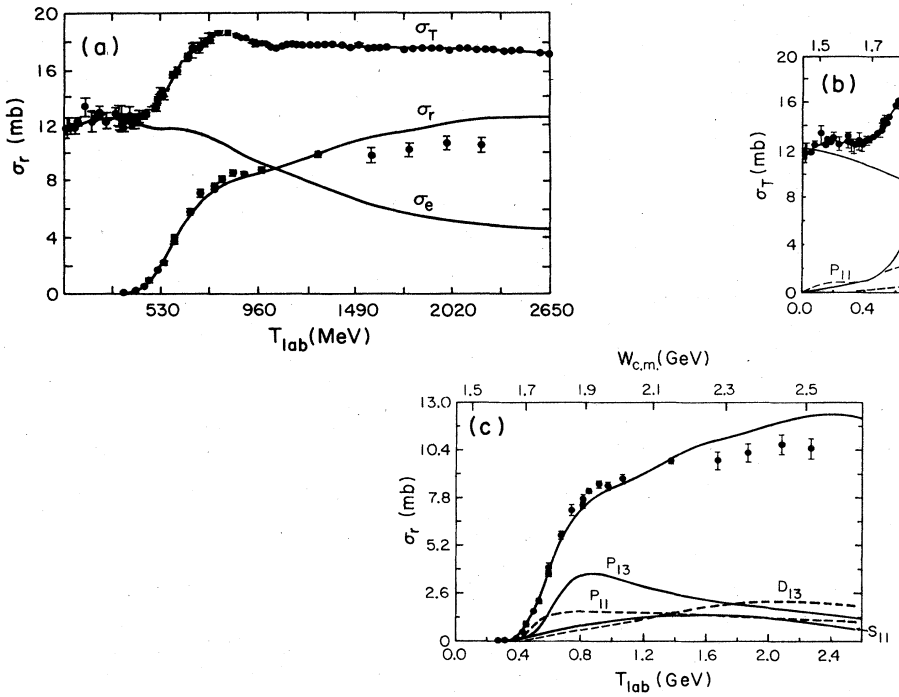

FIG. 4. Cross sections for our fit. (a) Our fit versus the total-cross-section σ_t and inelastic-cross-section σ_r data used in the fit. The calculated elastic-cross-section σ_e curve is also shown. (b) Total cross section and the most important of its partial-wave components. The $j=l+\frac{1}{2}$ partial waves are solid curves and the $j=l-\frac{1}{2}$ partial waves are dashed curves. (c) Inelastic cross section and its most important partial-wave components. The $j=l+\frac{1}{2}$ partial waves are solid curves and the $j=l-\frac{1}{2}$ partial waves are dashed curves.

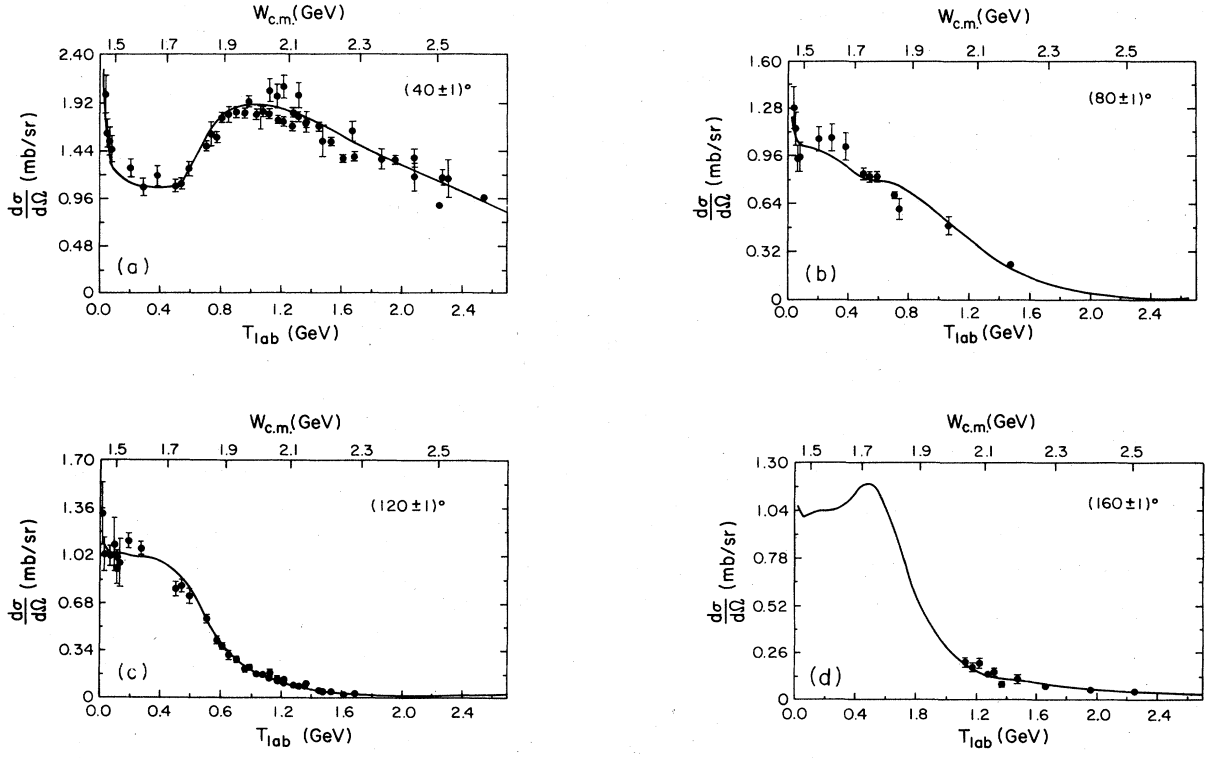

FIG. 5. Some representative differential cross-section data along with our energy-dependent solution's predictions. The different plots are for different center-of-mass scattering angles; the data are those within ±1° of the selected angle.

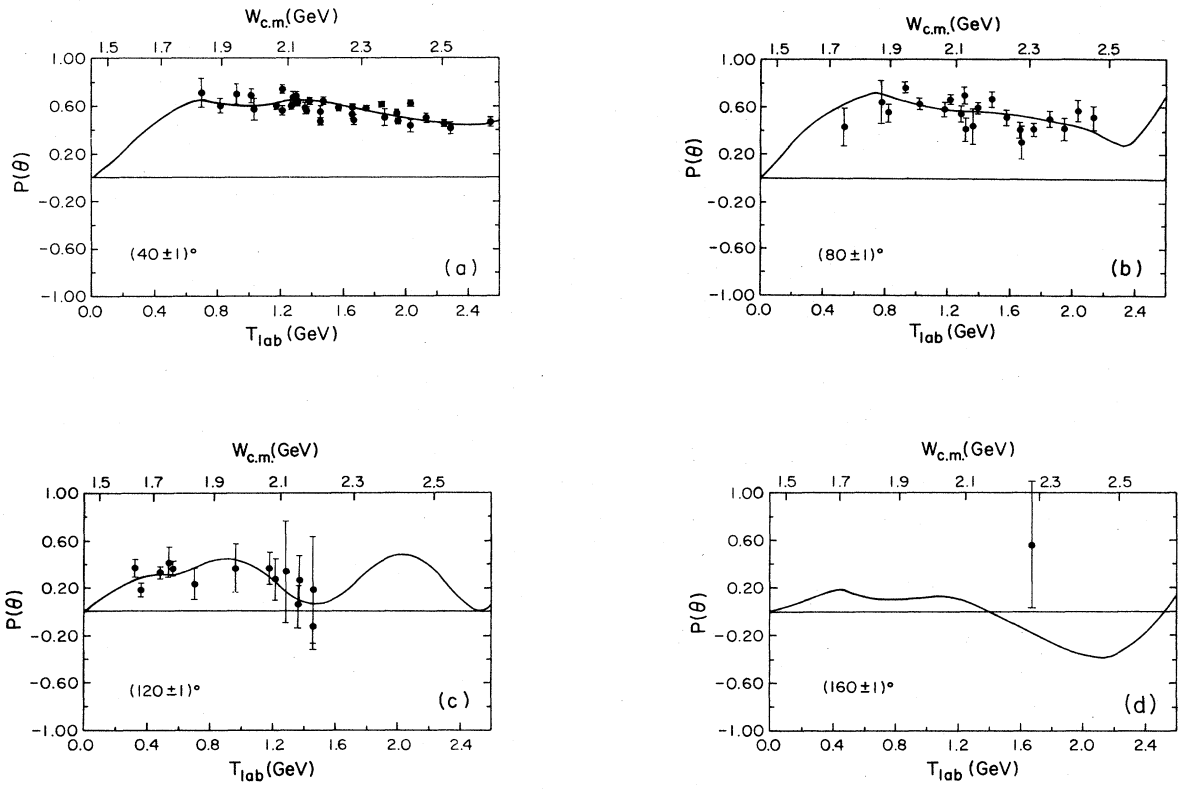

FIG. 6. Some representative polarization data along with our energy-dependent solution's predictions. The different plots are for different center-of-mass scattering angles; the data are those within $\pm 1°$ of the selected angle.

P_{13}, $(1680-i139)$ MeV ;

P_{11}, $(1735-i50)$ MeV ;

D_{15}, $(2054-i58)$ MeV .

The very rapid variation of the D_{15} partial wave [Fig. 8(a)] is due to two zeros flanking the pole; the higher zero is at $(2552-i100)$ MeV.

This occurrence of zeros near poles appears to be a common phenomenon for scattering systems; one can show that, in Schrödinger theory, a square well's poles are always accompanied by zeros, and our analyses of nucleon-nucleon and π-nucleon scattering also yield poles accompanied by nearby zeros (unpublished). Sometimes the zero lies behind or to the side of the pole relative to the real (physical) energy axis, and thus the pole is a dominant feature of the analytic structure (e.g., P_{13} and the D_{15}), but sometimes the zero lies in front of the pole, and thus the zero is the dominant feature (e.g., P_{11}). The P_{13}, D_{15}, and P_{11} resonances and related zeros are probably closely associated with the onset of inelastic cuts.

The poles and zeros accompanying them for the three resonances reported here are shown in contour and three-dimensional plots of the complex energy plane in Figs. 7–9 for our energy-dependent solution. In the three-dimensional plots the poles are cut off at different values for each partial wave in order that the surrounding structure can be seen.

VII. FUTURE WORK

To help those experimentalists who may be planning to measure spin-rotation parameters in the future, we include plots of

$$\beta=\arctan[2\,\mathrm{Re}(f^*g)/(|f|^2-|g|^2)]/\pi \tag{5}$$

in Fig. 10.

It appears that precise measurements of observables in the energy region near the P_{11} and P_{13} resonances (400–1100-MeV laboratory kinetic energy) would be useful in better defining the partial-wave amplitudes.

We are currently doing an $I=0$ and $I=1$ K^+N analysis up to 1100-MeV laboratory kinetic energy.

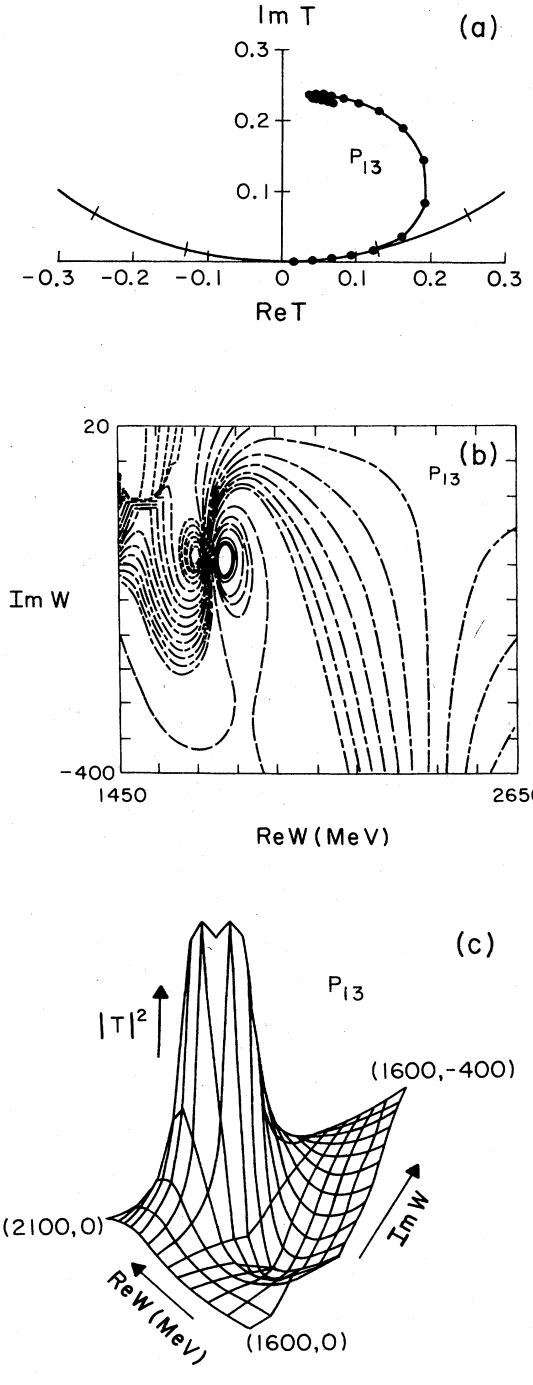

FIG. 7. P_{13} analytic structure. (a) Argand diagram. The dots indicate 50-MeV laboratory-kinetic-energy increments. (b) Contour plot of $|T|^2$ on the complex energy plane second sheet relative to the elastic cut. The inelastic cut runs to the left. The contour key is short dash=0—0.01 in units of 0.002; short-long dash=0.01—0.12 in units of 0.01; long dash=0.2—0.5 in units of 0.1; solid=1—2 in units of 0.5. Note the zero to the left of the pole. (c) Three-dimensional plot of complex energy plane. The pole is cut off at a value such that the nearby features are visible. Note the zero near the pole.

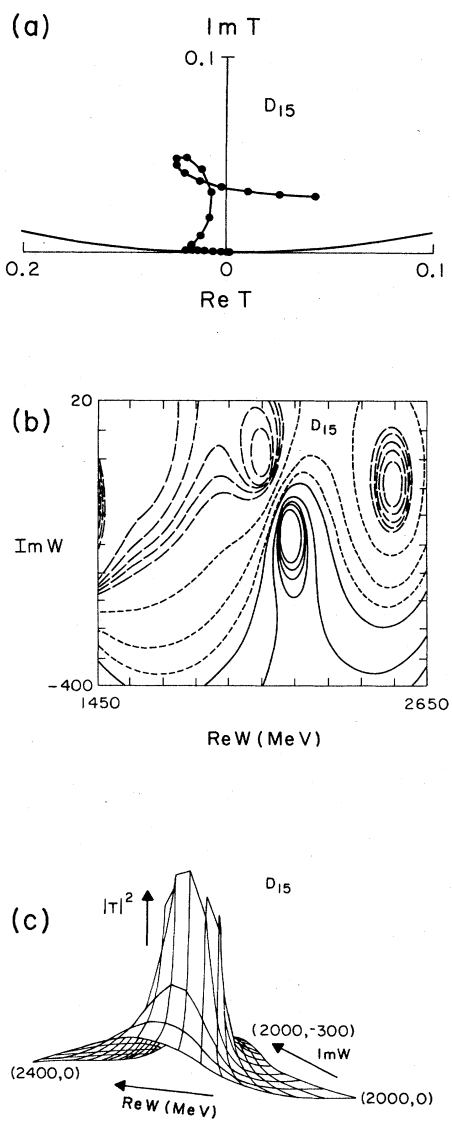

FIG. 8. D_{15} analytic structure. (a) Argand diagram. The dots indicate 50-MeV laboratory-kinetic-energy increments. (b) Contour plot of $|T|^2$ on the complex energy plane second sheet relative to the elastic cut. The contour key is long dash=0—0.001 in units of 0.0001; short dash=0.002—0.009 in units of 0.001; solid=0.01—0.06 in units of 0.01. Note the zero between the real axis and the pole, and a second zero near the end of the energy range. (c) Three-dimensional plot of complex energy plane. The pole is cut off at a value such that the nearby features are visible.

VIII. SCATTERING-ANALYSES INTERACTIVE DIAL-IN (SAID)

For the last several years the Center for Analysis of Particle Scattering in the Department of Physics at VPI&SU has made available an interactive dial-in computing system to any interested user. This system is called "SAID" for "scattering analyses interactive dial-

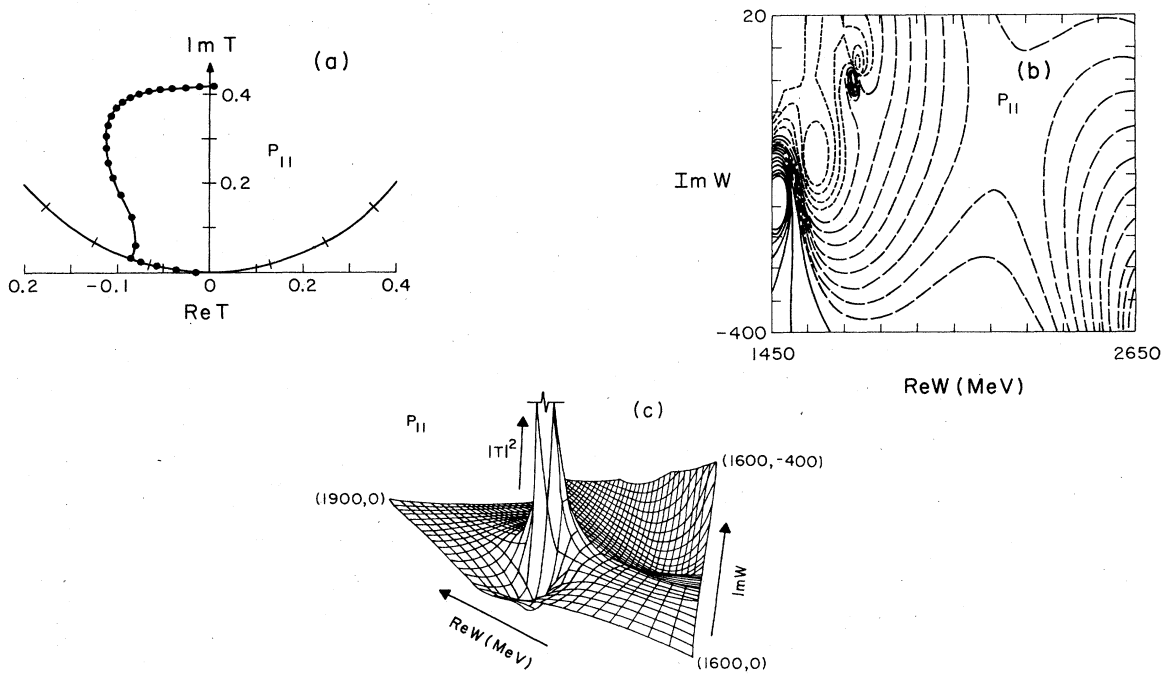

FIG. 9. P_{11} analytic structure. (a) Argand diagram. The dots indicate 50-MeV laboratory-kinetic-energy increments. (b) Contour plot of $|T|^2$ on the complex energy plane second sheet relative to the elastic cut. The contour key is short-dash=0—0.04 in units of 0.02; long dash=0.06—0.2 in units of 0.02; solid=0.25—0.5 in units of 0.05. Note the two zeros, each to the right-front of the two poles. (c) Three-dimensional plot of complex energy plane around the P_{11} pole. The pole is cut off at a value such that the nearby features are visible. Only the nearest pole is shown entirely. The two zeros are clearly visible.

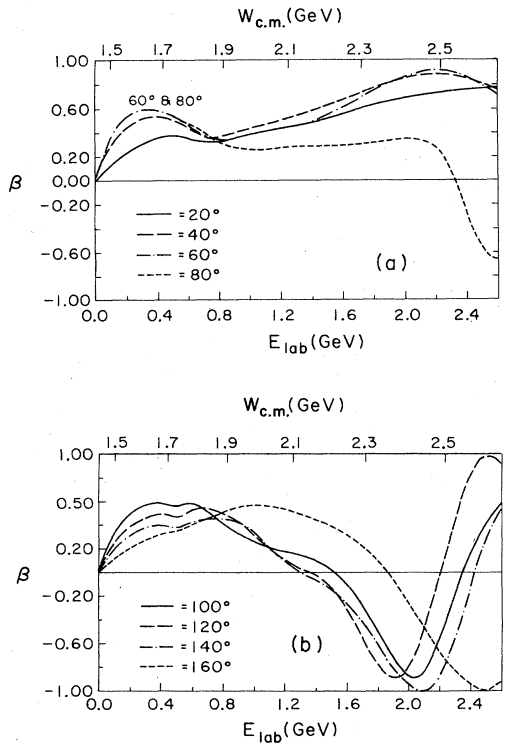

FIG. 10. Predictions of our solution for β [Eq. (5)] at selected angles versus energy.

in." SAID enables a user to dial into the VPI&SU computing system, using any type of terminal, in order to obtain a large amount of experimental and theoretical information about nucleon-nucleon, π-proton, and K^+-proton scattering below a few GeV.

SAID is a system for displaying the extant partial-wave solutions obtained from analyses of these reactions and for displaying the data bases from which the solutions were derived, along with the solutions' predictions of the observables. Other solutions besides ours are included. Users can also enter their own solutions and/or data and can conduct parameter studies. SAID can be used with any type of terminal; graphics output of amplitudes and observables is available on Tektronix compatible graphics terminals. Recently we added color graphics for the NEC APC microcomputer using the ESC140 VT100/Tektronix terminal emulator. A manual describing how to dial into and use SAID is available from the authors.

Recently, SAID has been converted to run on the VAX11-780/VMS system, and has been redesigned so that it can be sent by tape to sites other than VPI&SU. This eliminates the telephone charges and allows faster graphics. Other VAX/VMS users can obtain SAID at no cost by contacting the authors.

IX. CONCLUSION

From our investigation of the analytical structure of the partial wave amplitudes, we judge that the P_{13} resonance

is the best established of the three resonances claimed in this paper, followed by the D_{15} resonance, and the P_{11} resonance is the least well established.

We do not regard our results as precise determinations of parameters of the K^+p resonances, but do regard them as strong indicators of the existence of several resonances in the K^+p system. A more precise determination of the parameters awaits a better parametrization for energy-dependent analyses and/or more complete sets of data at strategic energies and angles. Our SAID computing system should be very helpful to experimentalists in determining which measurements would be most helpful and to theorists who are trying to understand the K^+-nucleon interaction or are using it to calculate K^+-nucleus interactions.

Our solution's S_{11} state indicates a possible resonance beyond the upper limit of our energy range. Angular data above our energy range would be desirable to investigate this possibility.

There has been considerable discussion in the literature[5] recently about resonances in exotic systems, such as the K^+p system, being "pseudoresonances" or "doorway" states. The contention is that such "resonances" are really due to logarithmic singularities caused by box diagrams rather than by simple poles. In this crude calculation a counterclockwise Argand loop occurs in every partial wave, thus masquerading as a "real" resonance. However, it is not clear that resonance poles do not occur when the "theory" is unitarized, which it must be in order to fit scattering data. We plan to allow such logarithmic singularities in the parametrizations of our future analyses of exotic systems.

In our future work on the K^+p system, we plan to try to devise other parametrizations for our energy-dependent fits and to apply tests to distinguish whether these K^+p resonances are real resonances or pseudoresonances. We are also equipped to aid experimentalists in determining the best observables, angles, and energies for future K^+p scattering experiments; either by their dialing into our SAID computing system at VPI&SU, or by our sending them the SAID system to use on their own VAX11-780/VMS computing system.

Because of the two resonances (P_{13} and P_{11}) we observe in the 400—1100-MeV laboratory-kinetic-energy region, it appears that precise measurement of observables in this region would be helpful.

Detailed tables of our solution are available through SAID or from the authors. A manual about how to use SAID by dialing into the VPI&SU computers is available from the authors.

ACKNOWLEDGMENTS

This work was sponsored by United States Department of Energy Contract No. DE-AS05-76-ER04928. The authors are grateful to a large number of colleagues who have made suggestions regarding these analyses and the SAID programs. We wish to thank Mr. Hossain Khoroosi for help in preparing this paper.

APPENDIX: ANALYTIC CALCULATION OF DISPERSION FUNCTION

The disperson function of Eq. (2) can be calculated analytically, as follows:

$$\pi C_l = \int_0^1 [x^{l+1/2}/(x-z)]dx \ , \tag{2}$$

a complex function, where

$$z=(W-W_t)/(W-W_z) \ ,$$

and the W's are defined in Eq. (2). One can show that C_l satisfies the recursion relation

$$\pi C_l = \pi z C_{l-1} + 1/(l+\tfrac{1}{2}) \tag{A1}$$

and that the lowest one is

$$\pi C_0 = \int_0^1 [x^{l+1/2}/(x-z)]dx$$
$$= 2+\sqrt{z}\,\ln[(1-\sqrt{z})/(1+\sqrt{z})]+i\pi\sqrt{z} \ . \tag{A2}$$

[1]R. A. Arndt, L. D. Roper, and P. H. Steinberg, Phys. Rev. D **18**, 3278 (1978).

[2]G. S. Abrams, L. Eisenstein, T. A. O'Halloran, Jr., W. Shufeldt, and J. Whitmore, Phys. Rev. Lett. **21**, 1407 (1968) (Ref. 68A1, differential cross sections at 2.76 GeV/c); J. Whitmore, G. S. Abrams, L. Eisenstein, J. Kim, T. A. O'Halloran, Jr., and W. Shufeldt, Phys. Rev. D **3**, 1092 (1971) (Ref. 71W1, differential cross sections at 2.53 and 2.76 GeV/c); J. A. Danysz, B. K. Penney, B. C. Stewart, G. Thompson, J. M. Brunet, J. L. Narjoux, N. J. D. Jacobs, P. H. Lewis, and P. V. March, Nucl. Phys. **B42**, 29 (1972) (Ref. 72D1, differential cross sections at 2.31 and 2.53 GeV/c).

[3]B. R. Martin, Nucl. Phys. **B94**, 413 (1975).

[4]B. J. Edwards and G. H. Thomas, Phys. Rev. D **22**, 2772 (1980); J. L. Basdevant and E. L. Berger, *ibid.* **19**, 239 (1979).

[5]I. M. Narodetskii and Y. A. Simonov, Yad. Fiz. **28**, 1356 (1978) [Sov. J. Nucl. Phys. **28**, 698 (1978)].